# Complex network approaches for epidemic modeling: a case study of COVID-19

Akhil Kumar Srivastav[1⋆], Vizda Anam[1,2], Rubén Blasco-Aguado[1],
Carlo Delfin S. Estadilla[1,5], Bruno V. Guerrero[1], Amira Kebir[3,4], Luís Mateus[1],
Bechir Naffeti[1], Fernando Saldaña[1], Vanessa Steindorf[1], and Nico Stollenwerk[1]

[1]BCAM-Basque Center for Applied Mathematics, Bilbao, Basque Country, Spain
[2]Department of Mathematics and Statistics, University of the Basque Country
(UPV/EHU), Leioa, Basque Country, Spain
[3]BIMS-IPT, University of Tunis El Manar, Tunisia
[4]IPEIT, University of Tunis, Tunisia
[5]Preventive Medicine and Public Health Department,
University of the Basque Country (UPV/EHU), Leioa, Basque Country, Spain

**Abstract.** Since the SARS-CoV-2 outbreak, the importance of mathematical modeling as a tool for comprehending disease dynamics has been highlighted, with several mathematical modeling techniques being applied and developed to simulate and measure the impact of interventions aimed at controlling the spread of the disease and minimizing its burden. In this work, we applied complex network techniques to analyze a Susceptible-Exposed-Asymptomatic-Hospitalized-Recovered (SEAHR) model to describe COVID-19 transmission dynamics, using the Basque Country region of Spain as a case study. We compared two network modeling approaches: the Watts-Strogatz network and the Barabasi-Albert scale-free network. By applying immunization strategies on both networks, we demonstrate that targeted immunization yields superior results within a scale-free network due to its increased heterogeneity. Moreover, the basic reproduction number of the model is calculated and sensitivity analysis is performed to determine the influence of the model parameters on the disease dynamics.

**Keywords:** Complex Network, Watts-Strogatz network, Scale-free network, COVID-19, Disease modeling, Targeted immunization policies.

## 1 Introduction

The spread of infectious diseases in animal and human populations is a continuous process that dates back to ancient times probably following the rise of agriculture [32]. Although there has been enormous progress in the understanding, prevention, and control of infectious diseases over the past century, the global burden remains high [7]. The SARS-CoV-2 pandemic raised awareness of

---

⋆ Corresponding Author.

the importance of mathematical models as a tool to understand disease dynamics better. Models were used successfully for forecasting the pandemic evolution, particularly hospital demand, and evaluating the impact of vaccines and non-pharmaceutical interventions [1–3,18]. The majority of epidemic models found in the literature are formulated as compartmental models based on the traditional Susceptible-Infectious-Recovered (SIR) model first proposed by Kermack and McKendrick [20]. Furthermore, it is usually assumed that host contact patterns follow the so-called mass action law or homogeneous mixing, so all hosts have identical contact rates within the population [25]. The homogeneous mixing of the entire population can be appropriate for outbreaks within small to medium size communities. Nevertheless, at a higher scale, for example, in multi-country epidemic outbreaks, there can be important heterogeneity in travel patterns and population distribution that can affect epidemic spread [14]. In other words, heterogeneity in host contact patterns can play a key role in disease dynamics and therefore it is important to develop models that include more details about individual-level interactions [5].

Recently, network-based models have been proposed to explicitly account for heterogeneity in host contact rates. Several studies have argued that contacts among individuals that allow the spread of an infectious disease naturally define a network and hence this network provides insight into the underlying epidemiological dynamics [5,12,31]. For instance, a compartmental network model was proposed in [33] to study COVID-19 in Wuhan and in the Great Toronto Area. The model was used to project new infections and the effect of the measures against the spread. Within network epidemic models, individuals are represented as nodes, and an edge between two nodes represents a contact with the potential to transmit the disease. Depending on the number of connections and their distribution among the nodes, different networks can be defined. In [13], the authors simulate the COVID-19 expansion in various regions with an extended SIR model adding a quarantine compartment, in order to try to find later the network that better fits that number of infections. Epidemiological models on networks have the potential to improve over mean-field descriptions of population dynamics with a better description of interactions among individuals. For example, while in standard compartmental models, the set of contacts is continually changing, network epidemic models usually assign to each individual a finite set of permanent contacts that can lead to infection [5,12,15,31]. Furthermore, even if individuals have the same number of connections in both homogeneous mixing and network models, the permanence of interactions in networks might cause a fast, localized outbreak, followed by a decreasing incidence once the susceptible class reduces locally [15]. Even though disease extinction often occurs in network models, if an outbreak arises, it is usually explosive [21].

A network is typically represented by a graph. A finite graph can be defined in terms of its adjacency matrix that describes the contacts among the individuals in the network. The graph can be undirected, directed, weighted, time-dependent, or combinations of these in order to reflect the biological or physical characteristics of the system under study [5,12,15,31]. Several network

formulations have been used to study the epidemic spreading process including random, lattice, small-world, and scale-free networks [15]. As the name suggests, in random networks the contacts among individuals are assigned at random. In lattice networks, individuals are the nodes in a regular grid, and contacts are established among adjacent individuals. So, lattice models are spatially localized and highly clustered. Small-world networks, also known as Watt-Strogatz (WS) networks [31], integrate characteristics from random and lattice networks by adding a certain number of random connections to a lattice [15, 31]. Barabasi-Albert (BA) scale-free networks, in turn, are a type of network in which the degree distribution follows a power law. The power law implies that the great majority of nodes have few connections, while a few important nodes (so-called hubs) have a huge number of connections [5, 12, 15, 31]. These differences may imply the necessity of using different vaccination strategies, as studied in [28], where they simulated a SAIRV model of COVID-19 in Italy with two vaccination methods in a random and in a BA scale-free network

Using differential equations, we present in this chapter a complex network model as a theoretical framework to investigate the epidemic spreading process of COVID-19 infection in the Basque Country, a region of Spain, as a case study. To this end, we employ a complex network technique to analyze a proposed Kermack-McKendrick-type model with a Susceptible-Exposed-Asymptomatic-Hospitalized-Recovered (SEAHR) structure. The SEAHR model is an extension of the well-known SIR framework in which the $I$ class is divided into two groups labeled $H$ and $A$: $H$ stands for individuals developing a severe form of the disease and likely being hospitalized, while $A$ refers to infected individuals who are asymptomatic or have a mild form of the disease. In this study, we focus on two network modeling approaches: the WS network and the BA scale-free network. In the next section, the underlying assumptions of the model are explained in detail. The mathematical properties of the model and the basic reproduction number are discussed in Section 3. Furthermore, a sensitivity analysis is implemented to determine the influence of various parameters on disease dynamics. The theoretical aspects of the network structure are discussed in Section 4. In Section 5, we analyze a number of immunization strategies under both WS and BA scale-free networks, aiming to better understand the trade-off between population heterogeneity and the effectiveness of targeted vaccination programs. A complete discussion of our results is given in Section 6.

## 2   Formulation of the complex network model

A compartmental complex network differential equation model focused on describing COVID-19 spreading features is formulated and analyzed. In contrast to classical compartmental models, here it is necessary to consider the interaction of each individual with their contact in the network. In this way, each individual in the community can be regarded as a vertex (node) in the network, and each contact between two individuals represented as an edge (line) connecting the

vertices. The number of edges originating from a vertex, that is the number of contacts a person has, is called the degree of the vertex.

In this work, we assume that the total population is divided into $n$ distinct groups of sizes $N_k$, $k = 1, 2, ..., n$, such that each individual in the group $k$ has exactly $k$ contacts per day. $S_k$, $E_k$, $A_k$, $H_k$ and $R_k$ denote the number of susceptible, exposed, asymptotically infectious, symptomatically-infectious (hospitalized) and recovered nodes at time $t$ and with degree $k$. Let $N_k(t) = S_k(t) + E_k(t) + A_k(t) + H_k(t) + R_k(t)$ represent the subtotal population with degree $k$ at time $t$. Then, the total population is denoted by $N = N_1 + N_2 + ... + N_n = \sum_{k=1}^{n} N_k$, and the probability that a uniformly chosen individual has $k$ contacts is $P(k) = \frac{N_k}{N}$. thus $N_k(t) = NP(k)$ . We also assume that the total human population $N$ is constant.

The proposed model is formulated considering the following assumptions:

1. Susceptible individuals, through their contacts get exposed to the infection, and move to the exposed class at rates $\beta$ and $\phi\beta$ if the effective contact was with a symptomatic/hospitalized or asymptomatic human individual, respectively. The factor $\phi > 1$, differentiates the force of infection among asymptomatic and symptomatic infections, meaning that asymptomatic individuals contribute more to the force of infection.
2. After the exposure period to the infection $\frac{1}{\zeta}$, a fraction $\eta$ develops severe symptoms and moves to the hospitalized class, while the remaining fraction $(1 - \eta)$ of exposed individuals that do not show any clinical symptoms move to the asymptomatic class.
3. Symptomatic/hospitalized individuals will get treatment and they will recover at a rate $\gamma_1$. However, due to some complications of the infection, some individuals will eventually die at a rate $\delta$.
4. We assume that asymptomatic individuals recover and they will move to the recovered class with a rate $\gamma_2$.
5. We will also assume, initially, that the recovery rate for symptomatic/hospitalized and asymptomatic will be the same, that is, $\gamma_1 = \gamma_2$, in order to simplify the assumptions and guarantee the symmetry between classes. However, biologically speaking, those rates can be different [10], and thus, this effect will be considered in the numerical simulations in the following sections.
6. Note that in the SARS-CoV-2 epidemic, asymptomatic people play a critical role in the spread of disease since they have no symptoms, have greater mobile, and encounter more people with a higher probability of infection compared to symptomatic individuals, who are possibly hospitalized or quarantined. Therefore, the symptomatic class and the asymptomatic class are differentiated in our model.

Considering these assumptions detailed before, the model can be represented by the following graph, (depicted in Figure 1), for each group $k$, of size $N_k$, having $k$ contacts:
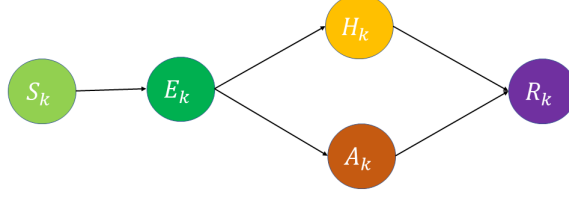
**Fig. 1.** Flow diagram of the model for a group $k$, proposed to represent the dynamic for COVID-19 infection via an SEAHR compartmental model.

And the ODE complex network model reads:

$$\frac{dS_k(t)}{dt} = -\beta\phi k S_k \theta_1(t) - \beta k S_k \theta_2(t)$$

$$\frac{dE_k(t)}{dt} = \beta k S_k[\phi\theta_1(t) + \theta_2(t)] - \zeta E_k(t)$$

$$\frac{dH_k(t)}{dt} = \eta\zeta E_k - \gamma_1 H_k(t) - \delta H_k(t) \tag{1}$$

$$\frac{dA_k(t)}{dt} = (1-\eta)\zeta E_k(t) - \gamma_2 A_k(t)$$

$$\frac{dR_k(t)}{dt} = \gamma_1 H_k(t) + \gamma_2 A_k(t)$$

where $\theta_1$ and $\theta_2$ are defined as follows:

$$\theta_1(t) = \frac{1}{\langle k \rangle}\sum_{k'=1}^{n} k' P(k') A_{k'}(t), \qquad \theta_2(t) = \frac{1}{\langle k \rangle}\sum_{k'=1}^{n} k' P(k') H_{k'}(t),$$

and

$$\langle k \rangle = \sum_{k'=1}^{n} k' P(k').$$

For the convenience of the reader, Table 1 depicts the parameters and their descriptions, as well as the baseline values used for the numerical simulations. The values were obtained from [1], where the data of COVID-19 from the Basque Country region of Spain was fitted to a modified SIR model, showing good agreement with the data and the model.

| Parameters | Description | Baseline values |
|---|---|---|
| $\beta$ | : infection rate | $3.25 \times \gamma_1 = 0.1625$ |
| $\zeta$ | : rate of becoming infectious after latency | 0.5 [2-5 days] |
| $\eta$ | : rate of becoming symptomatic/hospitalized infected | 0.45 [0-1] |
| $(1-\eta)$ | : rate of becoming asymptomatic infected | 0.55 [0-1] |
| $\gamma_1$ | : recovery rate for symptomatic/hospitalized individuals | $0.05d^{-1}$ |
| $\gamma_2$ | : recovery rate for asymptomatic individuals | $0.05d^{-1}$ |
| $\delta$ | : disease-related death for symptomatic/hospitalized individuals | $0.025d^{-1}[0.02-0.03]$ |
| $\phi$ | : ratio of mild/asymptomatic infections contributing to force of infection | 1.6 [1-2] |
| Constants | | |
| $N$ | : population size | $2.2 \times 10^6$ |
| $E(0)$ | : exposed initial population | 110 |
| $H(0)$ | : hospitalized initial population | 50 |
| $A(0)$ | : mild disease and asymptomatic initial population | 80 |
| $R(0)$ | : recover initial population | 1.0 |

**Table 1.** Baseline parameter values used for simulations. The baseline values were obtained from [1].

## 3   Analysis of the network model

### 3.1   Positivity of the solutions

For the proposed network model (1), we proved the positivity of the solutions.

**Theorem 1.** *The solutions $S_k(t)$, $E_k(t)$, $A_k(t)$, $H_k(t)$ and $R_k(t)$ of system (1) with initial conditions $S_k(0) > 0, E_k(0) \geq 0, A_k(0) \geq 0, H_k(0) \geq 0, R_k(0) \geq 0$, are positive for all $t > 0$.*

*Proof.* If $S_k(0) > 0$, according to the first equation of system (1), we have,

$$\frac{dS_k(t)}{dt} + \beta\phi k S_k(t)\theta_1(t) + \beta k S_k(t)\theta_2(t) = 0.$$

This can be rewritten as

$$\frac{dS_k(t)}{dt} exp\left\{\int_0^t (\beta\phi k\theta_1(\tau) + \beta k\theta_2(\tau))d\tau\right\}$$

$$+S_k(t)(\beta\phi k\theta_1(\tau) + \beta k\theta_2(\tau))exp\left\{\int_0^t (\beta\phi k\theta_1(\tau) + \beta k\theta_2(\tau))d\tau\right\} = 0.$$

That implies that

$$\frac{d}{dt}\left[S_k(t)exp\left\{\int_0^t (\beta\phi k\theta_1(\tau) + \beta k\theta_2(\tau))d\tau\right\}\right] = 0,$$

and then,

$$S_k(t)exp\left\{\int_0^t (\beta\phi k\theta_1(\tau) + \beta k\theta_2(\tau))d\tau\right\} - S_k(0) = C$$

with $C$ = constant.

As $S_k(0) > 0$ is a constant, we get

$$S_k(t)exp\left\{\int_0^t (\beta\phi k\theta_1(\tau) + \beta k\theta_2(\tau))d\tau\right\} =: C_1 \ (C_1 = \text{constant}).$$

Therefore, at $t = 0$ in the last equation, we get $S_k(0) = C_1$. Thus,

$$S_k(t)exp\left\{\int_0^t (\beta\phi k\theta_1(\tau) + \beta k\theta_2(\tau))d\tau\right\} = S_k(0) > 0.$$

Hence,

$$S_k(t) = S_k(0)exp\left\{-\int_0^t (\beta_1 k\theta_1(\tau) + \beta_2 k\theta_2(\tau))d\tau\right\} > 0.$$

Similarly, we can prove that $E_k(t) > 0$, $A_k(t) > 0$, $H_k(t) > 0$, $R_k(t) > 0$. Therefore, the solutions of system (1) with initial conditions $S_k(0) > 0, E_k(0) \geq 0, A_k(0) \geq 0, H_k(0) \geq 0, R_k(0) \geq 0$, are positive for all $t > 0$.

This completes the proof of Theorem 1.

Throughout this chapter, we will focus on the dynamics of the system (1) in the following bounded region:

$$\Omega = \{(S_1.....S_k, E_1......E_k, A_1......A_k, H_1.....H_k, R_1......R_k) : S_k > 0, E_k \geq 0, A_k \geq 0,$$
$$H_k \geq 0, R_k \geq 0, S_k + E_k + A_k + H_k + R_k = N_k, \}, \quad \text{where} \ \ 0 \leq k \leq n\}.$$

Also, all parameters are assumed to be positive. Their descriptions and baseline values are provided in Table 1.

### 3.2   The basic reproduction number

The system (1) has a unique disease-free equilibrium

$$E^0 = (N_1^0, ..., N_k^0, 0, ..., 0, 0, ..., 0, 0, ..., 0, 0, ..., 0).$$

Following the theory stated in [26, 29], we note that only the infectious compartments $E_k$, $H_k$ and $A_k$ are involved in the calculation of $\mathcal{R}_0$. In the disease-free state, $E^0$, the matrix whose entries are the rate of appearance of new infections, $F$, and the matrix whose entries are the rate of transfer of individuals out of the compartments, $V$, are given by

$$F = \begin{pmatrix} 0 & F_{12}^{n\times n} & F_{13}^{n\times n} \\ 0 & 0 & 0 \\ 0 & 0 & 0 \end{pmatrix}$$

where

$$F_{12}^{n \times n} = \frac{\beta S_k^0}{\langle k \rangle} \begin{pmatrix} 1P(1) & 2P(2) & \cdots & nP(n) \\ 2P(1) & 2 \cdot 2P(2) & \cdots & 2nP(n) \\ \vdots & \vdots & & \vdots \\ nP(1) & 2nP(2) & \cdots & n \cdot nP(n) \end{pmatrix},$$

$$F_{13}^{n \times n} = \frac{\phi \beta S_k^0}{\langle k \rangle} \begin{pmatrix} 1P(1) & 2P(2) & \cdots & nP(n) \\ 2P(1) & 2 \cdot 2P(2) & \cdots & 2nP(n) \\ \vdots & \vdots & & \vdots \\ nP(1) & 2nP(2) & \cdots & n \cdot nP(n) \end{pmatrix},$$

and

$$V = \begin{pmatrix} \zeta & 0 \cdots & 0 & 0 & \cdots & 0 & 0 \cdots & 0 \\ 0 & \zeta \cdots & 0 & 0 & \cdots & 0 & 0 \cdots & 0 \\ \vdots & \vdots & \vdots & \vdots & & \vdots & \vdots & \vdots \\ 0 & 0 \cdots & \zeta & 0 & \cdots & 0 & 0 \cdots & 0 \\ -\zeta\eta & 0 \cdots & 0 & \gamma_1 + \delta \cdots & 0 & 0 \cdots & 0 \\ \vdots & \vdots & \vdots & \vdots & & \vdots & \vdots & \vdots \\ 0 & 0 \cdots & -\zeta\eta & 0 & \cdots \gamma_1 + \delta & 0 \cdots & 0 \\ -(1-\eta)\zeta & 0 \cdots & 0 & 0 & \cdots & 0 & \gamma_2 \cdots & 0 \\ \vdots & \vdots & \vdots & \vdots & & \vdots & \vdots & \vdots \\ 0 & 0 \cdots & -(1-\eta)\zeta & 0 & \cdots & 0 & 0 \cdots & \gamma_2 \end{pmatrix}.$$

Therefore,

$$D = FV^{-1} = \begin{pmatrix} D_{11}^{n \times n} & D_{12}^{n \times n} & D_{13}^{n \times n} \\ 0 & 0 & 0 \\ 0 & 0 & 0 \end{pmatrix},$$

where

$$D_{11}^{n \times n} = \frac{1}{\langle k \rangle} \left[ \frac{\eta \beta S_k^0}{\gamma_1 + \delta} + \frac{\beta \phi (1-\eta) S_k^0}{\gamma_2} \right] \begin{pmatrix} 1P(1) & 2P(2) & \cdots & nP(n) \\ 2P(1) & 2 \cdot 2P(2) & \cdots & 2nP(n) \\ \vdots & \vdots & & \vdots \\ nP(1) & 2nP(2) & \cdots & n \cdot nP(n) \end{pmatrix},$$

$$D_{12}^{n \times n} = \frac{1}{\langle k \rangle} \left[ \frac{\beta S_k^0}{\gamma_1 + \delta} \right] \begin{pmatrix} 1P(1) & 2P(2) & \cdots & nP(n) \\ 2P(1) & 2 \cdot 2P(2) & \cdots & 2nP(n) \\ \vdots & \vdots & & \vdots \\ nP(1) & 2nP(2) & \cdots & n \cdot nP(n) \end{pmatrix},$$

and,

$$D_{13}^{n \times n} = \frac{1}{\langle k \rangle} \left[ \frac{\phi \beta S_k^0}{\gamma_2} \right] \begin{pmatrix} 1P(1) & 2P(2) & \cdots & nP(n) \\ 2P(1) & 2 \cdot 2P(2) & \cdots & 2nP(n) \\ \vdots & \vdots & & \vdots \\ nP(1) & 2nP(2) & \cdots & n \cdot nP(n) \end{pmatrix},$$

According to [26, 29], the basic reproduction number can be defined mathematically as the spectral radius of the matrix $FV^{-1}$. Therefore, we need to compute the eigenvalues of $FV^{-1}$. Note that the matrices $D$ and $D_{11}^{n \times n}$ have the same spectral radius, since $D$ is an upper triangular matrix.

Observe that the last $n - 1$ rows in the matrix $D_{11}^{n \times n}$ can be obtained as a linear combination of the first row. Hence, $D_{11}^{n \times n}$ has rank 1 and only one non-zero eigenvalue. Consequently, the spectral radius $\rho(D_{11}^{n \times n})$, is equal to the absolute value of the trace of $D_{11}^{n \times n}$.

Note that,

$$trace(D_{11}^{n \times n}) = \frac{\langle k^2 \rangle}{\langle k \rangle} \left[ \frac{\eta \beta}{\gamma_1 + \delta} + \frac{\beta \phi (1 - \eta)}{\gamma_2} \right] S_k^0.$$

Therefore, the basic reproduction number is given by

$$\mathcal{R}_0 = \frac{\langle k^2 \rangle}{\langle k \rangle} \left[ \frac{\eta \beta}{\gamma_1 + \delta} + \frac{\beta \phi (1 - \eta)}{\gamma_2} \right] S_k^0.$$

The term $\frac{\langle k^2 \rangle}{\langle k \rangle}$ denotes the average number of contacts. The term $\frac{\phi \beta (1 - \eta)}{\gamma_2} S_k^0$ denotes the expected number of asymptomatic individuals generated by a single asymptomatic infected human, and $\frac{\beta \eta}{(\gamma_2 + \delta)} S_k^0$ denotes the expected number of symptomatic / hospitalized individuals generated by a single symptomatic infected human. In this model, the basic reproduction number $\mathcal{R}_0$ denotes the number of secondary infected cases generated by a single infected case, in a region where the whole population under consideration is susceptible.

**Impacts of parameters on the basic reproduction number.** In order to visualize the impact of each parameter on the basic reproduction number, we apply the normalized forward sensitivity analysis technique. For that, we analyze the parameters affecting the basic reproduction number $\mathcal{R}_0$. The ratio of the relative change in the variable to the relative change in the parameter is indicated by the normalized forward sensitivity index of a variable to a parameter. Thus,

the forward sensitivity index is differentiable with regard to the parameter $\bar{p}$, which is defined by

$$\xi_{\mathcal{R}_0}^{\bar{p}} = \frac{\partial \mathcal{R}_0}{\partial \bar{p}} \cdot \frac{\bar{p}}{\mathcal{R}_0}. \tag{2}$$

This analytical expression for each parameter of the model can be easily calculated using the above equation, and thus, the sensitivity of $\mathcal{R}_0$ with respect to each parameter can be computed. The aim of this analysis is to find the key parameter that impacts the basic reproduction number the most, thus being the main driver in producing new infections and therefore, likely an outbreak. By finding the key parameter, it is possible to analyze which control measure is needed to decrease $\mathcal{R}_0$, and thus the spread of the disease.

Figure 2 shows the results of this analysis, taking into account the baseline values for the parameters set in Table 1. The transmission rate $\beta$ and the average size of the connection have a direct impact on the value of $\mathcal{R}_0$, and are also the key parameters that increase it. Additionally, the hospitalization rate, $\eta$, and the difference ratio between symptomatic and asymptomatic, $\phi$, are also directly correlated, albeit with a comparatively lower impact on $\mathcal{R}_0$.

Furthermore, the recovery rates $\gamma_1$ and $\gamma_2$ and the death rate $\delta$ exhibit an inverse relationship with $\mathcal{R}_0$. Thus, enhancing healthcare environments would significantly contribute to disease mitigation. Nevertheless, the size of connections remains to be the primary parameter exerting the most substantial impact. Hence, for respiratory diseases like COVID-19, effective disease control needs a reduction in both the number of contacts and the transmission rate.
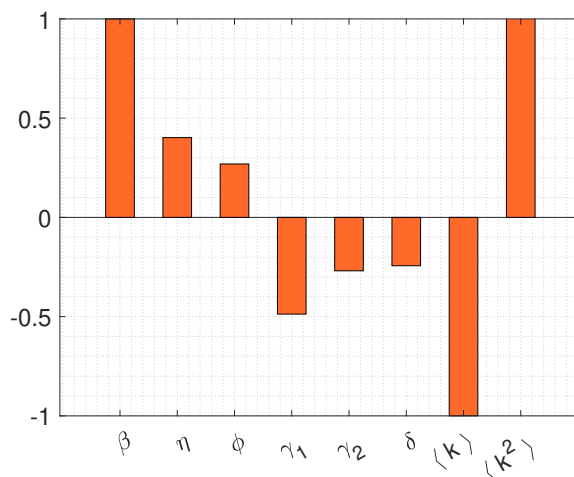


**Fig. 2.** Normalized forward sensitivity indices of $\mathcal{R}_0$ with respect to the parameters of the model. The baseline values of the model parameters are shown in Table 1.

Overall, the result shows that by adopting the above measures, the disease can be controlled. In Figure 3 we show the impact of combined control measures on $\mathcal{R}_0$. Figure 3(a) shows that if the transmission rate $\beta$ increases and the recovery rate $\gamma_1$ is kept at its lowest value (longer recovery time for symptomatic individuals), then the reproduction number $\mathcal{R}_0$ will increase, resulting in a very high number of infected individuals and an eventual outbreak.

Figure 3(b) meanwhile shows the impact of a combined strategy that includes the reduction of the transmission rate and control of the ratio of mild/asymptomatic infections contributing to the force of infection $\phi$. Our results suggest that disease mitigation can also be achieved, for instance, by increasing the detection rate among asymptomatic individuals or implementing curfew measures to curtail mobility.



(a)                                                                    (b)
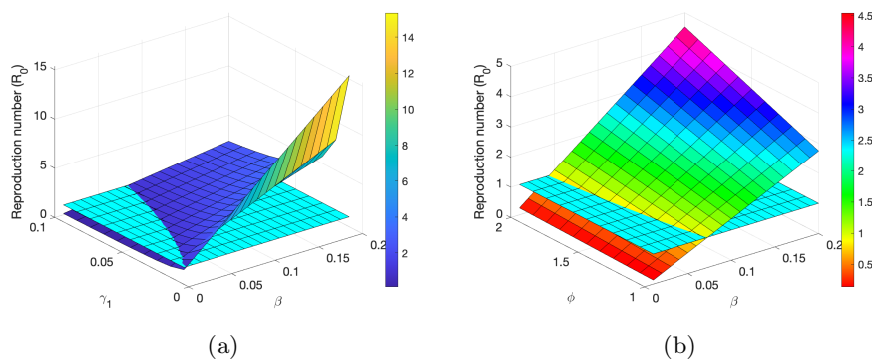
**Fig. 3.** Effect of applying different control measures on infection spread, via parameter analysis impact on $\mathcal{R}_0$. The baseline values of the model parameters are shown in Table 1. Here, $\beta$ and $\gamma_1$ vary from $[0, 0.2]$ and $[0, 0.1]$, respectively. The cyan plane represents $\mathcal{R}_0 = 1$.

Therefore, the threshold $\mathcal{R}_0$ is crucial in an epidemiological context for assessing the magnitude of an epidemic. This significance is further evidenced theoretically in the network model, as demonstrated in the next section (3.3), where we establish that the disease dies out when $\mathcal{R}_0 < 1$.

### 3.3   Stability analysis of the model

As a consequence of the results from [29], we can establish the local stability of the disease-free equilibrium:

**Theorem 2.** *If $\mathcal{R}_0 < 1$, the disease-free equilibrium*

$$E^0 = (N_1^0 ... N_k^0, 0..0, 0..0, 0..0, 0..0).$$

*of the system (1) is locally asymptotically stable, and if $\mathcal{R}_0 > 1$, the disease-free equilibrium $E^0$ is unstable.*

Furthermore, we prove a more general result of global stability.

**Theorem 3.** *If $\mathcal{R}_0 < 1$, the disease-free equilibrium*

$$E^0 = (N_1^0...N_k^0, 0..0, 0..0, 0..0, 0..0).$$

*of the system (1) is globally asymptotically stable whenever the eigenvalues of the matrix $F - V$ have a negative real part. And, if $\mathcal{R}_0 > 1$, the disease-free equilibrium $E^0$ is unstable.*

*Proof.* This theorem is proved using the comparison theorem [16]. Using the same notation as in [26], and re-writing the equations for the exposed and infected compartments of the system (1) we get

$$
\begin{pmatrix} E_1 \\ E_2 \\ \vdots \\ E_n \\ H_1 \\ H_2 \\ \vdots \\ H_n \\ A_1 \\ A_2 \\ \vdots \\ A_n \end{pmatrix} = (F-V) \begin{pmatrix} E_1 \\ E_2 \\ \vdots \\ E_n \\ H_1 \\ H_2 \\ \vdots \\ H_n \\ A_1 \\ A_2 \\ \vdots \\ A_n \end{pmatrix} - \begin{pmatrix} \phi\beta S_1\theta_1(t) + \beta S_1\theta_2(t) \\ 2\phi\beta S_2\theta_1(t) + 2\beta S_2\theta_2(t) \\ \vdots \\ k\phi\beta S_k\theta_1(t) + k\beta S_k\theta_2(t) \\ 0 \\ 0 \\ \vdots \\ 0 \\ 0 \\ \vdots \\ 0 \end{pmatrix}.
$$

If all the eigenvalues of the matrix $F - V$ have negative real parts, the system is stable for $\mathcal{R}_0 < 1$. By the comparison theorem [16], it follows that

$$(E_1, E_2.......E_k, H_1, H_2.......H_k, A_1, A_2.......A_k,) \to (0, 0.....0, 0, 0....0, 0, 0....0)$$

as $t \to \infty$. Then $(E_1, E_2.......E_k, H_1, H_2.......H_k, A_1, A_2.......A_k,) \to E^0$ as $t \to \infty$. Therefore, $E^0$ is globally asymptotically stable for $\mathcal{R}_0 < 1$.

## 4   Network model dynamics

Network models have been useful in describing dynamics in real-world contexts such as social networks [23], neuroscience [6], and metabolism [34]. In this chapter, we aim to apply approaches in network modeling to the epidemiological model proposed herein. Specifically, we will create a WS network [31] and analyze the role that this network structure plays in the model structure. Moreover, we will connect the nodes via a BA scale-free network [5] and compare the two complex structures.

### 4.1   A WS network

A WS network is characterized by a small-world graph with random features, such as clustering and a low average path length. The following steps describe how a small-world network with $N$ nodes can be built:

1. Create a regular lattice with $N$ nodes of average degree $2K$. Each node is connected to its $K$ nearest neighbors, $K$ vertices clockwise and $K$ counter-clockwise.
2. Each edge in the graph, with independent and uniform probability $\hat{p}$, is removed and replaced by a new edge between two nodes that are chosen uniformly, at random, from the $N$ nodes, without duplicating or self-looping edges.

   For instance, when $\hat{p} = 0$, a ring graph in which each node is coupled to its $K$ nearest neighbors is obtained as shown in Figure 4(a). While, when $\hat{p} = 0.1$, the result is a random graph, as shown in Figure 4($b$). The topology of a small-world network is illustrated in Figure 4, for $N = 20$, $K = 2$ and two different wiring probabilities.



(a) $\hat{p} = 0$                                    (b) $\hat{p} = 0.1$
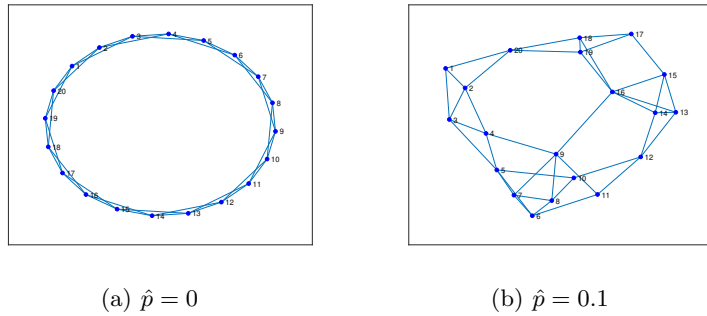
**Fig. 4.** WS small-world network with $N = 20$, $K = 2$ (the average degree is 4) and the wiring probabilities are, in (a) $\hat{p} = 0$, and in (b) $\hat{p} = 0.1$.

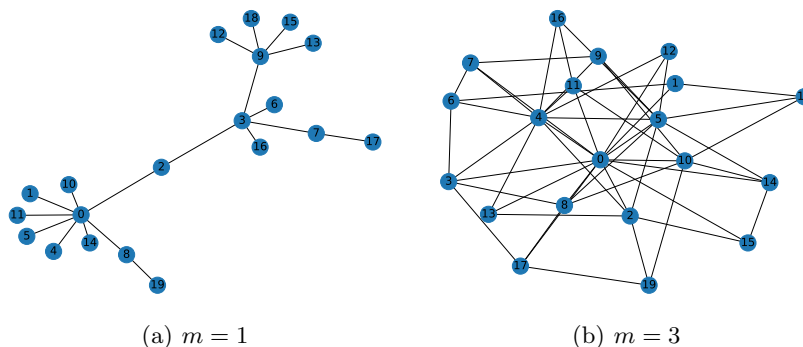### 4.2   A BA scale-free network

The BA scale-free networks are represented by the scenario of a few hubs with high connection and most nodes with low connectivity, as shown in Figure 5. The following algorithm produces an undirected BA scale-free network of size $N$:

1. Start with an initial network of size $m_0$. Then $N - m_0$ nodes are introduced sequentially into the network, where each node connects with $m^* \leq m_0$ existing nodes.

Note that it is typical to choose $m^* = m_0$ and it is not possible to choose $m^* > m_0$ since the first new node introduced cannot be assigned $m^*$ edges. Thus, the initial network with size $m_0$, will determine the maximum average degree of the network.

2. The $m^*$ connections of the new node with the existing ones are chosen with a probability that is proportional to their current degree. More than one edge between two nodes is not allowed. Thus, the combination of network growth with this preferential attachment is what leads to a power-law degree distribution.

In this chapter, we adapted the algorithm described in [27], according to the study described in [24]. The topology of a BA scale-free network is illustrated in Figure 5 for $N = 20, m_0 = 3$ and two different preferential attachment values $m = 1$ and $m = 3$, in Figure 5 (a) and (b), respectively.



(a) $m = 1$                                    (b) $m = 3$

**Fig. 5.** BA scale-free network, with $N = 20, m_0 = 3$, and in (a) $m = 1$ and in (b) $m = 3$.

### 4.3   Comparison of the two network structures

Here, we compare the results of applying both networks to the model (1). For that, we define degree distribution for each of the networks. The "degree distribution" is defined as the probability distribution of the number of nodes and connections across the network. When the probability distribution resembles a "Power Law", then the network is called "scale-free", or a "power law" network, where $P(k) = k^{-\eta}$ and $2 < \eta < 3$.

The WS structure starts with a ring of $N$ vertices in which each vertex is connected to its $2m_1$ nearest neighbors. Afterwards, each edge can be reconnected to a different node with probability $\hat{p}$, and preserved with probability $1 - \hat{p}$. Consequently, the degree distribution is the following expression approximated by a Poisson distribution:

$$P(k) = \sum_{k=0}^{\min(k-m_1,m_1)} \binom{m_1}{n} (1-\hat{p})^n \hat{p}^{m_1-n} \frac{\hat{p}m_1^{k-m_1-n}}{(k-m_1-n)!} e^{-\hat{p}m_1} \qquad (3)$$

and as $\hat{p} \to 1$,

$$P(k) = \frac{m_1^{k-m_1}}{(k-m_1)!} e^{-m_1}.$$

We now compare the behavior of model (1) for both the WS network with degree distribution described in equation (3) and for the BA scale-free network with a power law distribution. The numbers for the total asymptomatic, $\sum_{k=0}^{n} A_k$, total hospitalized $\sum_{k=0}^{n} H_k$, and total infected population, $\sum_{k=0}^{n}(A_k + H_k)$ are shown in Figure 6. The results show that applying the WS network to represent the contact in each group will produce a higher number of infected individuals than applying the BA scale-free network to represent the contact between individuals of the same group.
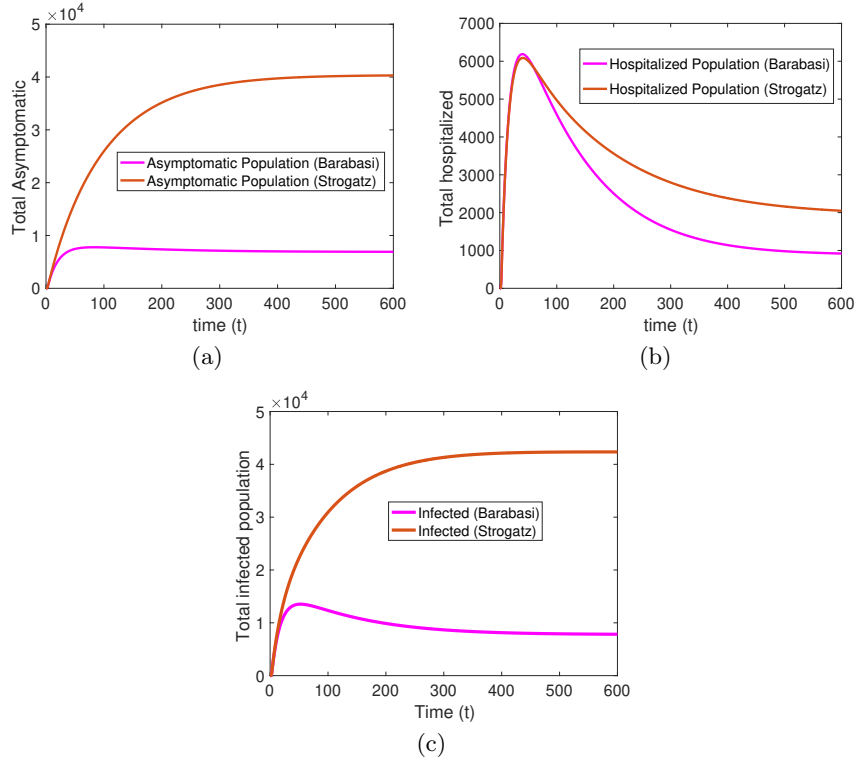


**Fig. 6.** Comparison of the solution of the model (1) by applying two network structures to represent the contacts. The baseline values of the model parameters are shown in Table 1.

## 5   Control and immunization

### 5.1   Uniform immunization strategy

The uniform immunization strategy is the simplest immunization scheme [22]. In order to get a uniform immunization density, it is assumed that immune nodes cannot become infected and, thus, do not transmit the infection to their neighbors. In this case, for a fixed infection rate $\beta$, the fraction of immune nodes present in the network denoted $p$ can be a relevant quantity to take as a control parameter. At the mean-field level, the presence of uniform immunity will effectively reduce the spreading rate $\beta$ by a factor $(1-p)$. Considering the existence of the immunized fraction $(0 < p < 1)$, the model (1) now reads as

$$
\begin{aligned}
\frac{dS_k(t)}{dt} &= -(1-p)\beta\phi k S_k \theta_1(t) - (1-p)\beta k S_k \theta_2(t) \\
\frac{dE_k(t)}{dt} &= (1-p)\beta k S_k[\phi\theta_1(t) + \theta_2(t)] - \zeta E_k(t) \\
\frac{dH_k(t)}{dt} &= \eta\zeta E_k - \gamma_1 H_k(t) - \delta H_k(t) \\
\frac{dA_k(t)}{dt} &= (1-\eta)\zeta E_k(t) - \gamma_2 A_k(t) \\
\frac{dR_k(t)}{dt} &= \gamma_1 H_k(t) + \gamma_2 A_k(t).
\end{aligned}
\tag{4}
$$

The effect of the control parameter $p$, on total infected cases $\sum_{k=0}^{n} A_k + H_k$, it is shown in Figure 7. In homogeneous networks, such as the WS model, the effect of uniform immunization strategy has a great impact in decreasing infection, see Figure 7(a). That is, a public policy of immunization of individuals, that allows total protection against infection and therefore against spreading, implies that in this kind of network, individuals have less chance of getting infected, allowing the protection of the network and reducing the spread of the infection.

On the other hand, the uniform immunization program is not so effective in reducing infections in a context where contacts resemble a BA scale-free network. The BA scale-free network is a heterogeneous network and a uniform immunization strategy cannot protect higher-order degree infected nodes, see Figure 7(b).
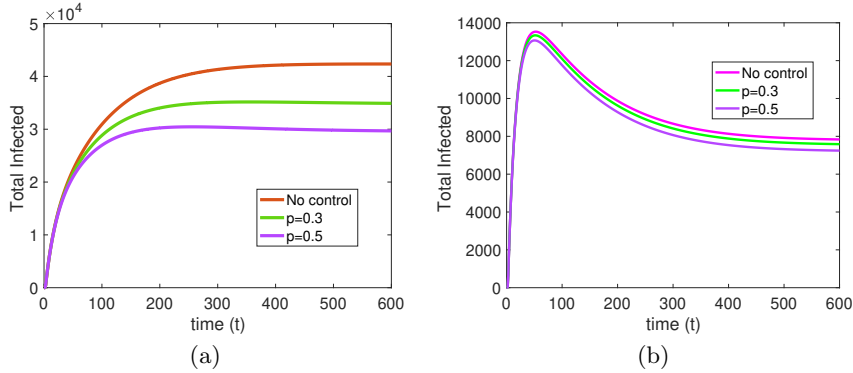
**Fig. 7.** Effect of the control parameter $p$ on total infected cases $\sum_{k=0}^{n}(A_k + H_k)$. Contacts are described by the WS model in (a) and the BA scale-free network in (b). The baseline values of the model parameters are shown in Table 1.

### 5.2 Optimized immunization strategies

When fighting an epidemic in a heterogeneous population with a uniform vaccination scheme, it is necessary to vaccinate a fraction of the population larger than the estimate given by a simple (homogeneous) assumption. In this case, it can be proved that optimal vaccination programs can eradicate the disease by vaccinating a smaller number of individuals. BA scale-free networks can be considered as a limiting case for heterogeneous systems, and it is natural for this case to apply another specifically devised immunization strategy. In the following, we describe another type of immunization that can be applied to BA scale-free networks.

**Targeted immunization** Another effective strategy is targeted immunization [22]. The very peculiar nature of the BA scale-free networks allows us to define more efficient strategies based on the nodes' hierarchy. In particular, it has been shown that BA scale-free networks possess a noticeable resilience to random connection failures, which implies that the network can resist a high level of damage to disconnected links, without losing its global connectivity properties.

In our network model (1), we introduce a lower and an upper threshold, $k_1$ and $k_2$, respectively, such that, if $k > k_2$, all nodes with connectivity $k$ are immunized, while if $k_1 < k < k_2$, then, $m_k \ (0 < m_k \leq 1)$ portion will be immunized. Therefore, defining $\eta_k$ as the fraction of individuals to be immunized, we have

$$\eta_k = \begin{cases} 1, & \text{if } k > k_2. \\ m_k, & \text{if } k_1 < k < k_2. \\ 0, & \text{if } k < k_1. \end{cases} \tag{5}$$

where $\hat{\eta} = \sum_k \eta_k P(k)$ is the average immunization rate. Applying this target immunization to the epidemic model (1) we have

$$\frac{dS_k(t)}{dt} = -(1 - \eta_k)\beta\phi k S_k \theta_1(t) - (1 - \eta_k)\beta k S_k \theta_2(t)$$

$$\frac{dE_k(t)}{dt} = (1 - \eta_k)\beta k S_k[\phi\theta_1(t) + \theta_2(t)] - \zeta E_k(t)$$

$$\frac{dH_k(t)}{dt} = \eta\zeta E_k - \gamma_1 H_k(t) - \delta H_k(t) \qquad (6)$$

$$\frac{dA_k(t)}{dt} = (1 - \eta)\zeta E_k(t) - \gamma_2 A_k(t)$$

$$\frac{dR_k(t)}{dt} = \gamma_1 H_k(t) + \gamma_2 A_k(t)$$

The analysis of this model is now performed. The basic reproduction number for this model is

$$\hat{\mathcal{R}}_0 = \frac{\langle k^2(1 - \eta_k)\rangle}{\langle k\rangle}\left[\frac{\eta\beta}{\gamma_1 + \delta} + \frac{\beta\phi(1 - \eta)}{\gamma_2}\right].$$

Rewriting it in terms of the basic reproduction number for the model without immunization (1), we get

$$\hat{\mathcal{R}}_0 = \mathcal{R}_0 - \left[\frac{\eta\beta}{\gamma_1 + \delta} + \frac{\beta\phi(1 - \eta)}{\gamma_2}\right]\frac{\langle k^2\eta_k\rangle}{\langle k\rangle},$$

which means that the number of new infections is reduced by a fraction of individuals who were immunized.

It is known that if a few of the most connected nodes are removed, in the context of BA scale-free networks, the network suffers a dramatic reduction of its ability to carry information [4,8]. Applying this strategy to the case of epidemic models, the targeted immunization scheme is the recommended immunization strategy in the case where the transmission resembles BA scale-free networks. Therefore, by applying this scheme, the immunization control affects the most highly connected nodes, i.e., the ones more likely to spread the disease.

Figure 8 shows that BA scale-free networks are strongly affected by the strategy of target immunization when selective damage on disconnected links occurs. In contrast, the WS network remains unaffected, indicating that target immunization does not exert control over the disease spread in this network type, unlike the uniform immunization strategy.

In Figure 8(b), the effect of control parameter $m_k$ can be seen, i.e., the portion of the node to be immunized, on the total infected cases, $\sum_{k=0}^{n}(A_k + H_k)$, on the BA scale-free network. The strategy is very effective in reducing the number of infected cases when $m_k$ is increasing. On the other hand, the number of infected cases in the WS network is not so effective in reducing spreading (see Figure 8(a)), since that network has the same number of connections with each infected node, and, in this case, the most highly connected nodes cannot be
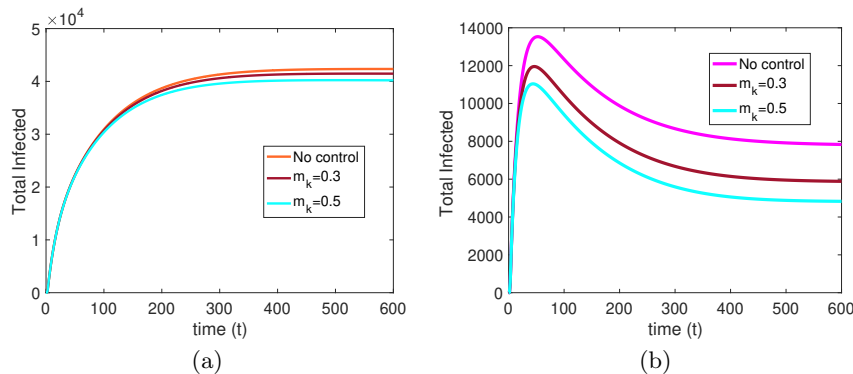
**Fig. 8.** Effect of the control parameter $\eta_k$, the proportion of individuals that will be immunized, on total the infected cases, $\sum_{k=0}^{n}(A_k + H_k)$. In (a) for WS network, in (b), for BA scale-free network. The baseline values of the model parameters are shown in Table 1.

found. Therefore, the above strategy is very beneficial in a BA scale-free network reducing infection in the population.

### 5.3 Impact of recovery rates on disease prevalence

In this section, we explore the impact of recovery rates, $\gamma_1$ and $\gamma_2$, on infected populations $\sum_{k=0}^{n} H_k$, $\sum_{k=0}^{n} A_k$ and on the overall infections $\sum_{k=0}^{n}(A_k + H_k)$, using both WS and BA scale-free networks. The effects will be analyzed numerically, and the results are presented in Figure 9.

In Figure 9(a) and (b), we vary the value of $\gamma_1$ value in both network models. The result shows that by increasing the recovery rate $\gamma_1$, the total hospitalized population decreases. A parallel analysis was conducted for the parameter $\gamma_2$. Here, we can also see that by increasing the value of $\gamma_2$, the total asymptomatic population decreased, see Figure 9(c) and (d).

Finally, Figure 9(e) and (f) shows the combined effect of varying both recovery rates, $\gamma_1$ and $\gamma_2$, on the total infected population, $\sum_{k=0}^{n}(A_k + H_k)$. Consistently, higher values of the recovery rate lead to a decrease in the total number of infections. Notably, there are no discernible differences in the impact of these values when evaluating the WS (left-side figures) and BA scale-free networks (right-side figures).

Certainly, augmenting medical facilities and treatments, and other actions that contribute to an increased recovery rate among individuals, will result in a reduction in disease spread. This approach has been used as an extension of the analysis of the difference in impact depending on the network applied.
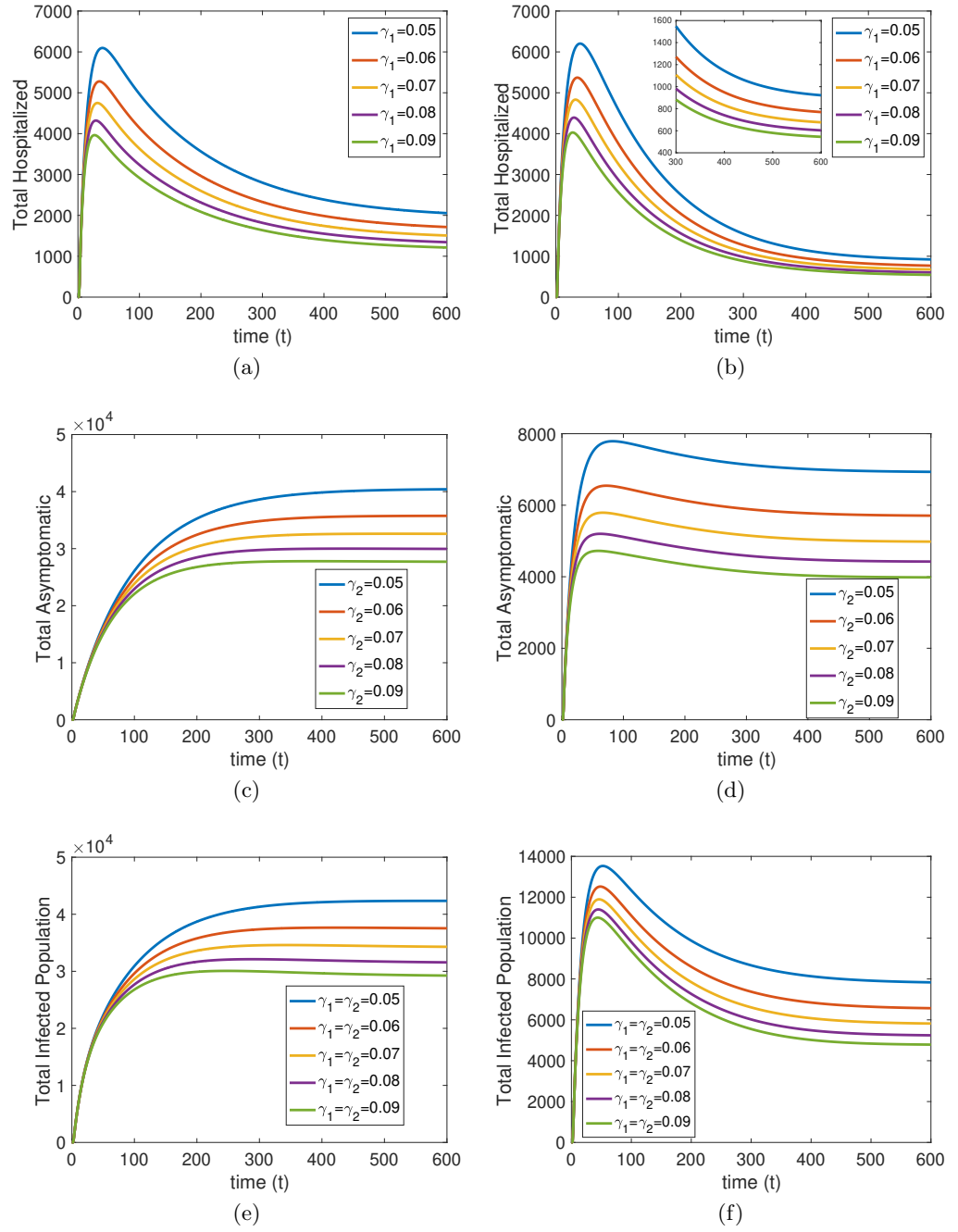
**Fig. 9.** Effect of the recovery rates in the numbers of infected population $\sum_{k=0}^{n} A_k$, $\sum_{k=0}^{n} H_k$ and $\sum_{k=0}^{n}(A_k + H_k)$, in the WS model (left-side panels), and the BA scale-free network model (right-side panels). The baseline values of the model parameters are shown in Table 1.

# 6 Discussion and conclusion

Mathematical models played a critical role in understanding the epidemiological dynamics of the spread and prevention measures of COVID-19 around the world [35]. However, many of these models assume homogeneous mixing in the population, implying that all individuals have the same number of contacts. This assumption may hold for smaller or more local areas, but using approaches that assume heterogeneity may allow for more realistic descriptions of disease dynamics in larger settings [30].

In this work, complex network techniques were used to propose and analyze a susceptible-exposed-hospitalized/symptomatic-asymptomatic-recovered (SEAHR) mathematical model for COVID-19 transmission specific to the Basque Country region of Spain. Our findings shed light on the effectiveness of different immunization strategies within the context of two network assumptions: the WS network and the BA scale-free network.

The results demonstrate that a uniform immunization strategy is more effective in a WS network, characterized by increased homogeneity, while a targeted immunization strategy performs better in a BA scale-free network, which exhibits greater heterogeneity. This difference underlines the impact of population heterogeneity on the effectiveness of vaccination programs. In the context of diseases with a notably heterogeneous spread, as observed in COVID-19 due to the presence of superspreaders [19], our results suggest that a targeted vaccination would be more effective in curtailing infections and hospitalizations.

Additionally, we calculated the basic reproduction number, $\mathcal{R}_0$, and analyzed the disease-free equilibrium of the SEAHR model. Through sensitivity analysis, we identified key parameters that significantly aid disease containment. Primarily, the results support the implementation of interventions that will decrease the transmission rate, $\beta$, hospitalization rate, $\eta$, and the relative infectiousness of mild/asymptomatic individuals, $\phi$. On the other hand, increasing the recovery rates, $\gamma_1$, and $\gamma_2$, possibly through improved treatment methods, will also reduce the disease impact.

It is important to note that our study focused on a specific complex network (mean field equation). Various approaches to network modeling exist, as demonstrated by previous works (e.g., [9, 11, 17]). While we focused on two specific approaches, the BA scale-free network is considered one of the more practical and tractable methods in network modeling [5, 28]. Future research could explore alternative network generation methods generalizing the quite restrictive generic networks due to their analytical tractability which we consider here and refine the COVID-19 model to incorporate additional factors such as reinfection dynamics, stratification by comorbidity and age, and immunity waning from vaccination, among others.

In conclusion, this work contributes to the understanding of COVID-19 dynamics through network modeling. Our analysis of immunization strategies under different network assumptions highlights the impact of population heterogeneity on the effectiveness of targeted vaccination programs. By using parameter values specific to the Basque Country region, we reinforce the significance

of interventions such as social distancing and use of mask in controlling disease transmission.

# References

1. Aguiar, M., Ortuondo, E.M., Bidaurrazaga Van-Dierdonck, J., Mar, J., Stollenwerk, N.: Modelling COVID 19 in the Basque Country from introduction to control measure response. Scientific Reports **10**(1), 17306 (Oct 2020). https://doi.org/10.1038/s41598-020-74386-1, `https://www.nature.com/articles/s41598-020-74386-1`

2. Aguiar, M., Van-Dierdonck, J.B., Mar, J., Cusimano, N., Knopoff, D., Anam, V., Stollenwerk, N.: Critical fluctuations in epidemic models explain COVID-19 post-lockdown dynamics. Scientific Reports **11**(1), 13839 (Jul 2021). https://doi.org/10.1038/s41598-021-93366-7, `https://www.nature.com/articles/s41598-021-93366-7`

3. Aguiar, M., Van-Dierdonck, J.B., Stollenwerk, N.: Reproduction ratio and growth rates: Measures for an unfolding pandemic. PLOS ONE **15**(7), e0236620 (Jul 2020). https://doi.org/10.1371/journal.pone.0236620, `https://dx.plos.org/10.1371/journal.pone.0236620`

4. Albert, R., Jeong, H., Barabási, A.L.: Error and attack tolerance of complex networks. Nature **406**(6794), 378–382 (Jul 2000). https://doi.org/10.1038/35019019, `https://www.nature.com/articles/35019019`

5. Barabási, A.L., Pósfai, M.: Network Science. Cambridge University Press, Cambridge, United Kingdom (2016)

6. Bassett, D.S., Sporns, O.: Network neuroscience. Nature Neuroscience **20**(3), 353–364 (Feb 2017). https://doi.org/10.1038/nn.4502, `https://doi.org/10.1038/nn.4502`

7. Bernstein, A.S., Ando, A.W., Loch-Temzelides, T., Vale, M.M., Li, B.V., Li, H., Busch, J., Chapman, C.A., Kinnaird, M., Nowak, K., Castro, M.C., Zambrana-Torrelio, C., Ahumada, J.A., Xiao, L., Roehrdanz, P., Kaufman, L., Hannah, L., Daszak, P., Pimm, S.L., Dobson, A.P.: The costs and benefits of primary prevention of zoonotic pandemics. Science Advances **8**(5), eabl4183 (Feb 2022). https://doi.org/10.1126/sciadv.abl4183, `https://www.science.org/doi/10.1126/sciadv.abl4183`

8. Callaway, D.S., Newman, M.E.J., Strogatz, S.H., Watts, D.J.: Network Robustness and Fragility: Percolation on Random Graphs. Physical Review Letters **85**(25), 5468–5471 (Dec 2000). https://doi.org/10.1103/PhysRevLett.85.5468, `https://link.aps.org/doi/10.1103/PhysRevLett.85.5468`

9. Calvetti, D., Hoover, A.P., Rose, J., Somersalo, E.: Metapopulation Network Models for Understanding, Predicting, and Managing the Coronavirus Disease COVID-19. Frontiers in Physics **8**, 261 (Jun 2020). https://doi.org/10.3389/fphy.2020.00261, `https://www.frontiersin.org/article/10.3389/fphy.2020.00261/full`

10. CDC: Isolation and precautions for people with covid-19, `https://www.cdc.gov/coronavirus/2019-ncov/your-health/isolation.html`

11. Chang, S., Pierson, E., Koh, P.W., Gerardin, J., Redbird, B., Grusky, D., Leskovec, J.: Mobility network models of COVID-19 explain inequities and inform reopening. Nature **589**(7840), 82–87 (Jan 2021). https://doi.org/10.1038/s41586-020-2923-3, `https://www.nature.com/articles/s41586-020-2923-3`

12. Danon, L., Ford, A.P., House, T., Jewell, C.P., Keeling, M.J., Roberts, G.O., Ross, J.V., Vernon, M.C.: Networks and the Epidemiology of Infectious Disease. Interdisciplinary Perspectives on Infectious Diseases **2011**, 1–28 (2011). https://doi.org/10.1155/2011/284909, `http://www.hindawi.com/journals/ipid/2011/284909/`

13. Dimou, A., Maragakis, M., Argyrakis, P.: A network sirx model for the spreading of covid-19. Physica A: Statistical Mechanics and its Applications **590**, 126746 (2022). https://doi.org/https://doi.org/10.1016/j.physa.2021.126746, `https://www.sciencedirect.com/science/article/pii/S0378437121009456`
14. Humphries, R., Mulchrone, K., Tratalos, J., More, S.J., Hövel, P.: A systematic framework of modelling epidemics on temporal networks. Applied Network Science **6**(1), 23 (Dec 2021). https://doi.org/10.1007/s41109-021-00363-w, `https://appliednetsci.springeropen.com/articles/10.1007/s41109-021-00363-w`
15. Keeling, M.J., Eames, K.T.: Networks and epidemic models. Journal of The Royal Society Interface **2**(4), 295–307 (Sep 2005). https://doi.org/10.1098/rsif.2005.0051, `https://royalsocietypublishing.org/doi/10.1098/rsif.2005.0051`
16. Lakshmikantham, V., Leela, S., Martynyuk, A.A.: Stability analysis of nonlinear systems. Springer International Publishing Switzerland 2015 **447**(7142), 279–283 (January 2016). https://doi.org/10.1007/978-3-319-27200-9, `https://link.springer.com/book/10.1007/978-3-319-27200-9`
17. Loyal, J.D., Chen, Y.: Statistical Network Analysis: A Review with Applications to the Coronavirus Disease 2019 Pandemic. International Statistical Review **88**(2), 419–440 (Aug 2020). https://doi.org/10.1111/insr.12398, `https://onlinelibrary.wiley.com/doi/10.1111/insr.12398`
18. Maíra, A., Vizda, A., Nicole, C., Damián, K., Nico, S.: Understanding COVID-19 Epidemics: A Multi-Scale Modeling Approach. Springer, Birkhäuser, Cham, Birkhäuser, printed edn. (2022)
19. Majra, D., Benson, J., Pitts, J., Stebbing, J.: SARS-CoV-2 (COVID-19) superspreader events. Journal of Infection **82**(1), 36–40 (Jan 2021). https://doi.org/10.1016/j.jinf.2020.11.021, `https://doi.org/10.1016/j.jinf.2020.11.021`
20. McKendrick, A.G.: A contribution to the mathematical theory of epidemics. Proceedings of the Royal Society of London. Series A, Containing Papers of a Mathematical and Physical Character **115**(772), 700–721 (Aug 1927). https://doi.org/10.1098/rspa.1927.0118, `https://royalsocietypublishing.org/doi/10.1098/rspa.1927.0118`
21. Naug, D., Choe, J.C.: Disease Transmission and Networks. In: Encyclopedia of Animal Behavior, pp. 801–806. Elsevier (2019). https://doi.org/10.1016/B978-0-12-809633-8.20875-3, `https://linkinghub.elsevier.com/retrieve/pii/B9780128096338208753`
22. Pastor-Satorras, R., Vespignani, A.: Immunization of complex networks. Physical Review E **65**(3), 036104 (Feb 2002). https://doi.org/10.1103/PhysRevE.65.036104, `https://link.aps.org/doi/10.1103/PhysRevE.65.036104`
23. Pomeroy, C., Bond, R.M., Mucha, P.J., Cranmer, S.J.: Dynamics of social network emergence explain network evolution. Scientific Reports **10**(1) (Dec 2020). https://doi.org/10.1038/s41598-020-78224-2, `https://doi.org/10.1038/s41598-020-78224-2`
24. Prettejohn, B.J., Berryman, M.J., McDonnell, M.D.: Methods for Generating Complex Networks with Selected Structural Properties for Simulations: A Review and Tutorial for Neuroscientists. Frontiers in Computational Neuroscience **5** (2011). https://doi.org/10.3389/fncom.2011.00011, `http://journal.frontiersin.org/article/10.3389/fncom.2011.00011/abstract`
25. Saldaña, F., Velasco-Hernández, J.X.: Modeling the COVID-19 pandemic: A primer and overview of mathematical epidemiology. SeMA Journal **79**(2), 225–251 (Jun 2022). https://doi.org/10.1007/s40324-021-00260-3, `https://link.springer.com/10.1007/s40324-021-00260-3`

26. Srivastav, A.K., Yang, J., Luo, X., Ghosh, M.: Spread of Zika virus disease on complex network—A mathematical study. Mathematics and Computers in Simulation **157**, 15–38 (Mar 2019). https://doi.org/10.1016/j.matcom.2018.09.014, `https://linkinghub.elsevier.com/retrieve/pii/S0378475418302465`

27. Tapan: Scale free network using B-A algorithm (Jul 2023), `https://mathworks.com/matlabcentral/fileexchange/49356-scale-free-network-using-b-a-algorithm`

28. Tetteh, J.N., Nguyen, V.K., Hernandez-Vargas, E.A.: Network models to evaluate vaccine strategies towards herd immunity in COVID-19. Journal of Theoretical Biology **531**, 110894 (Dec 2021). https://doi.org/10.1016/j.jtbi.2021.110894, `https://linkinghub.elsevier.com/retrieve/pii/S0022519321003131`

29. Van Den Driessche, P., Watmough, J.: Reproduction numbers and sub-threshold endemic equilibria for compartmental models of disease transmission. Mathematical Biosciences **180**(1-2), 29–48 (Nov 2002). https://doi.org/10.1016/S0025-5564(02)00108-6, `https://linkinghub.elsevier.com/retrieve/pii/S0025556402001086`

30. Wagner, C.E., Saad-Roy, C.M., Grenfell, B.T.: Modelling vaccination strategies for COVID-19. Nature Reviews Immunology **22**(3), 139–141 (Mar 2022). https://doi.org/10.1038/s41577-022-00687-3, `https://www.nature.com/articles/s41577-022-00687-3`

31. Watts, D.J., Strogatz, S.H.: Collective dynamics of 'small-world' networks. Nature **393**(6684), 440–442 (Jun 1998). https://doi.org/10.1038/30918, `https://www.nature.com/articles/30918`

32. Wolfe, N.D., Dunavan, C.P., Diamond, J.: Origins of major human infectious diseases. Nature **447**(7142), 279–283 (May 2007). https://doi.org/10.1038/nature05775, `https://www.nature.com/articles/nature05775`

33. Xue, L., Jing, S., Miller, J.C., Sun, W., Li, H., Estrada-Franco, J.G., Hyman, J.M., Zhu, H.: A data-driven network model for the emerging COVID-19 epidemics in Wuhan, Toronto and Italy. Mathematical Biosciences **326**, 108391 (Aug 2020). https://doi.org/10.1016/j.mbs.2020.108391, `https://linkinghub.elsevier.com/retrieve/pii/S0025556420300730`

34. Yilmaz, L.S., Walhout, A.J.: Metabolic network modeling with model organisms. Current Opinion in Chemical Biology **36**, 32–39 (Feb 2017). https://doi.org/10.1016/j.cbpa.2016.12.025, `https://doi.org/10.1016/j.cbpa.2016.12.025`

35. Zhang, W., Liu, S., Osgood, N., Zhu, H., Qian, Y., Jia, P.: Using simulation modelling and systems science to help contain COVID-19: A systematic review. Systems Research and Behavioral Science **40**(1), 207–234 (Aug 2022). https://doi.org/10.1002/sres.2897, `https://doi.org/10.1002/sres.2897`